SPE 81048

Characterising Reservoir Performance for the Mahogany 20 Gas Sand Based on Petrophysical and Rock Typing Methods

J. Ali-Nandalal, bpTT LLC, G. Gunter, NExT

This paper was prepared for presentation at the SPE Latin American and Caribbean Petroleum Engineering Conference held in Port-of-Spain, Trinidad, West Indies, 27–30 April 2003.

Abstract

The Mahogany Field in Trinidad produces ~475 MMscfd and is the sole supplier of the gas to Atlantic Liquefied Natural Gas (LNG) plant's train 1. The Mahogany Field's gas reserves are dedicated to the LNG plant. The original reserve calculations assumed volumetric depletion would be the dominant drive mechanism for the gas reservoirs in this field.

Four years later, water drive is the dominant drive mechanism for all sands except the 20 Sand. If the 20 Sand eventually shows water drive, the predicted rate profile and reservoir management would be different than if it had been a volumetric reservoir.

This study investigates both drive mechanisms and makes recommendations for managing the reservoir in either eventuality. To support this work, a petrophysical description was carried out. This included rock typing of the reservoir and calibrating the wireline log data with 20 Sand core. Three independent methods for rock typing were employed, two of which have not been used on offshore Trinidad core samples previously. A facies description was compared to the rock type classifications and flow units.

A reservoir simulation model was built using log analysis from the 20 Sand and incorporating the results of the petrophysical descriptions of the different rock types and flow units.

A history match was obtained for the well currently draining this reservoir and predictions on the 20 Sand incorporating a future 7" horizontal gas well were also done. The recovery factors were obtained for the reservoir under different drive mechanisms – volumetric and water drive. Recommendations for optimal reservoir management of the 20 Sand are given.

Introduction

The Mahogany field is located 61 miles offshore from the southeastern point of the island of Trinidad (Figure 1) in 300 ft of water. The field was discovered in the late 1960s and early 1970s. However, it was not developed due to lack of a gas market. Exploratory drilling in 1994 and 1996 discovered additional gas and condensate reserves. Mahogany's reserves were dedicated to the proposed Atlantic Liquefied Natural Gas plant at Point Fortin[1]. In early 1996 delineation wells (EM-5 and 5x) encountered additional gas reserves in the 20 Sand in the middle of the field. The original reserve calculations assumed volumetric depletion would be the dominant drive mechanism for the gas reservoirs in this field.

Four years and 714 Bscf later, water drive is the dominant drive mechanism for all sands except the 20 Sand. Water handling capacity is limited on the platform. Therefore, if the 20 Sand eventually shows water drive, the predicted rate profile and reservoir management would be different than if it had been a volumetric reservoir.

This paper describes the work done to develop a history-matched reservoir model and to predict production performance.

Geology/Reservoir Characterisation

The Mahogany Field, located in the Columbus Basin within the Eastern Venezuelan Basin, is a faulted anticlinal structure with Pliestocene age stacked sand and shale sequences. There are 15 reservoirs in the field, with over 2 Tscf in gas reserves. The 20 Sand (Figure 2) accounts for 26% of the total field's gas reserves. Estimated original gas in place is 814 Bscf, located in fault blocks IV and V. The productive area is approximately 4 miles long and 2 miles wide.

The 20 Sand is a northeasterly progradation of the Orinoco Delta in Pleistocene time. It consists of stacked "bow-tie" shaped[2] coarsening-upward sand sequences (Figure 3) interpreted to be mid-upper shoreface deposits interbedded with shales and silts. High rate of sediment, contemporaneous normal faulting, active regional tectonics and sea level change all contribute to the shape of these sequences. Four major stratigraphic units (Figure 4) extending over the 20 Sand

reservoir have been identified based on five wells and 3-D seismic. The stratigraphic units form part of the larger framework for flow unit description and reservoir model layers.

A 3-D seismic survey, acquired in 1993 specifically for field development, was used for structural mapping. The 20 Sand exhibits an anomalous, high-amplitude signature due to the presence of gas. However, individual stratigraphic units within the 20 sand reservoir are not resolvable.

Rock Typing

The 20 Sand reservoir consists of excellent reservoir rocks (Table 1). Core porosities and permeabilites average 32% and 2400 mD respectively. An iterative workflow was used to identify and confirm rock types, calibrate log data with core data and define flow units (Figure 5).

A 60 ft core, representing 20% of the 279 ft (measured depth) gross 20 Sand thickness, was obtained from the MA12 well (Figure 4). The logs used to calibrate to core data were bulk density, neutron porosity, gamma ray and resistivity. The electrical properties measured on the core indicated that cementation exponent m, and saturation exponent n, were 1.75 and 1.74, respectively.

Four petrophysical rock types were identified using three different porosity-permeability methods: the Pittman Crossplot[3], Cumulative Distribution Function[4, 5] and the Flow Zone Indicator methods described by Amaefule et al.[6]

The Pittman method, traditionally used to identify rock types in offshore Trinidad reservoirs, revealed four rock type classifications (Figure 6). These petrophysical rock types are identified on the Pittman cross plot of core porosity, permeability and pore throat isopore lines that reflect a particular pore geometry. It is an empirical method (Equation 1).

$$\log R30 = 0.215 + 0.547 \log(k_{air}) - 0.42 \log(\phi) \quad (1)$$

where R30 is the 30th percentile isopore radius (μm), k_{air} is core permeability to air in mD and ϕ is core porosity in percent.

This study is the first application of the Cumulative Distribution Function (CDF) to classify rock types in an offshore Trinidad reservoir. The CDF is a mathematical method used to calculate the probability of finding a random variable (in this case, permeability) that is less than or equal to a stipulated value. The permeability values are arranged in ascending order and the probabilities are calculated. Figure 7 shows that this method identified four rock types associated with the four distinct slopes on the graph.

This was also the first application of the Amaefule et al. Flow Zone Indicator (FZI) Method on an offshore Trinidad reservoir. Two different techniques were used to obtain FZIs. One method required calculating the Rock Quality Index (RQI in equation 2) for the core samples, which was plotted against a porosity function ϕ_Z (Equation 3) to obtain FZIs.

$$RQI = 0.314 (k/\phi)^{-0.5} \quad (2)$$

$$\phi_Z = \phi/(1-\phi) \quad (3)$$

where k is core permeability in μm^2 and ϕ is core porosity as a fraction.

The other method used core permeability (in μm^2) plotted against a porosity function ϕ_R (equation 4) to derive the FZIs.

$$\phi_R = \phi^3/(1-\phi)^2 \quad (4)$$

where ϕ is core porosity as a fraction. Both techniques classified four rock types (Figure 8A, B). While Flow Zone Indicators are excellent for rock typing, they do not represent continuous, stratigraphic units.

High-pressure mercury injection capillary data confirmed pore geometry and rock types. Further, nuclear magnetic resonance testing was used to investigate pore bodies, and laser particle size distribution confirmed textural properties (grain size and sorting) of the rock types distinguished by the methods above.

Seven facies were identified in the 20 Sand core, and Figure 9 shows that, with the exception of Facies 1, there is no one-to-one relationship between rock type and facies. The seven facies, identified by interpreting the primary sedimentary structures preserved in the slabbed core, were confirmed with the high-resolution formation image logs.

Facies 1 – Parallel to sub-parallel bedding
Facies 2 – Horizontal burrows
Facies 3 – Heavily bioturbated and disturbed bedding
Facies 4 – Thin laminated silts/shales and sands
Facies 5 – Massive sandstones
Facies 6 – Clean parallel sandstones or low angle cross laminations
Facies 7 – Shaley sandstones with laminations

Interpreters commonly use facies as the basis for constructing reservoir models in these types of young sediments. Intrinsic properties based on facies often are used for reservoir flow predictions. If the facies method were used in this case, it would result in poorer reservoir performance. For example, Facies 2, 3 and 4 show a wide range in permeability at a given porosity. Thus, an average permeability computed based on facies would be influenced by the lower values.

It is also clear that a high percentage of the core was classified as rock types 1 and 2. Therefore, the majority of the reservoir is capable of storing and transmitting fluids at high rates. Figure 10 shows the facies in terms of the Pittman plot. This further confirms that each rock type is generally composed of a range of facies.

Flow Units

The workflow for rock typing to flow unit delineation is shown in Figure 5. The method involves using a stratigraphic Modified Lorenz[7] plot (%kh versus %phih) and had successfully defined flow units in another Mahogany sand in a previous study.[8]

The steps are summarized below:

1. Used Pittman Plot to classify core porosity and permeability data into rock types as a first pass.
2. Selected plugs for coherent plug analysis to verify rock types using high-pressure mercury injection (pore throats), nuclear magnetic resonance (pore bodies) texture and grain size (laser particle size distribution) and mineralogy (quartz/feldspars/ lithics).
3. Using lab results in Step 2, confirmed and refined rock type classifications with Pittman plot, CDF and Amaefule et al. methods.
4. Using rock types, porosity, permeability and thickness, identified flow units on stratigraphic modified Lorenz plot (Figure 11) from core data.
5. Calibrated log-derived water saturation with irreducible water saturation from capillary pressure data (Figure 12).
6. Calibrated log-derived effective porosity with core porosity (Figure 13).
7. Calibrated log derived shale volume with laser particle size distribution clay fraction (Figure 14).
8. Used core permeability to calibrate a permeability prediction model based on log derived effective porosity and shale volume using a non-parametric spreadsheet add-in.[9, 10]
9. Used model from Step 8 to predict permeability for core data that was not used to build it, as an independent test (Figure 15).
10. Compared permeability model generated in Step 8 with permeability predicted by Timur and Coates equations that use porosity and irreducible water saturation as input. Selected best permeability prediction model.
11. Calculated upscaled flow units from log data for cored well over entire sand and compare with flow units from core.
12. With model from Step 8, used log-derived effective porosity and shale volume to predict permeability in the other wells.
13. Performed rock typing on other wells and used rock types, porosity, permeability and thickness to distinguish flow units on stratigraphic modified Lorenz plot.
14. Correlated flow units in all the wells and calculated average properties (thickness, porosity, permeability, water saturation) for each flow unit as input for reservoir simulation.

Reservoir Engineering

A material balance was performed prior to reservoir simulation. Gas initially in place was estimated at 449 Bscf, which was within 5% of the volumetrically derived value of 429 Bscf. The recovery factor from material balance was estimated at 59% at an abandonment pressure of 2000 psi. This high abandonment pressure ensured that, under current conditions, the tubing head pressure (THP) was at least 1000 psi for delivery to the liquefied natural gas plant, located 100 miles away. Figure 16 shows the P/Z versus cumulative gas production. The straight line indicates that volumetric depletion was the dominant reservoir drive mechanism to date. Recovery factor from material balance increases to 73% if compression is available, which lowers the abandonment pressure to 1300 psi (300 psi THP). The relatively high limit for abandonment pressure under compression avoids wellbore collapse, indicated to occur at 1210 psi by thick-wall cylinder tests.

A scoping reservoir simulation model was used to obtain a history match for the well currently draining the reservoir. To integrate the petrophysical and engineering data, the following were input into a multiphase flow simulator: (1) the flow units along with their average petrophysical properties (porosity, permeability, net-to-gross ratio, connate water saturation, relative permeability data, rock compressibilities) and (2) measured PVT (pressure-volume-temperature) fluid properties. While each flow unit had distinct average petrophysical properties, the model that represented the reservoir was a layercake type, with each layer representing a different flow unit. The structural data was simplified to one average sand top value. The relative permeability curve for a rock type 2 sample was used to represent all rock types.

To maintain the history match achieved for volumetric depletion, a weak aquifer was modeled for the water drive case.

Results/Discussion

Figures 17A, B, C and D show that a good pressure match was achieved for volumetric depletion as well as for a weak water drive. The condensate rate was slightly underpredicted.

The model predicted no water production, whereas an average of 20 bwpd had been produced for the last four years. This is within the range for water of vapourisation. The water-gas relative permeability curve (Figure 18) indicates that, for a small increase in water saturation, a large decrease in gas relative permeability occurs. Therefore, if the aquifer were stronger than the one modeled, a decrease in recovery factor would be anticipated.

The recovery factors for volumetric and water drive under current operating conditions were 53% and 56%, respectively, at an abandonment pressure of 2000 psi. Introducing a 7" horizontal well in the reservoir is expected to rate accelerate reserves by 3.7 years under volumetric depletion and 4 years under weak water drive (Table 2). If compression is introduced, then the abandonment pressure can be reduced to 1300 psi (300 psi THP). The recovery factors with compression for volumetric and weak water drive would increase to 70% and 72%, respectively.

Water drive increased predicted reserves in the 20 Sand because a weak aquifer was modeled. The aquifer support slowed down the rate of pressure decline so more reserves could be produced before the abandonment pressure was reached. However, the model did not predict increasing water

cuts with the attendant negative impacts of trapped gas saturation, higher abandonment pressures and water handling issues necessitating shutting in the wells earlier than planned. This incremental recovery due to water drive has been reported in another gas reservoir.[11]

The rate acceleration anticipated with the horizontal well would be enhanced with an additional well in the reservoir. This would allow faster withdrawal should it become necessary to outrun the water and would also reduce the risk associated with having only two high-rate wells depleting one reservoir.

Conclusions

1. Rock typing using three different methods classified the Mahogany 20 Sand into four different rock types. These rock types were confirmed by measurements of pore geometry and texture.
2. There is no one-to-one relationship between rock type and facies.
3. A scoping reservoir model incorporating average flow unit properties was built to predict performance of the 20 Sand reservoir in Fault Block IV of the Mahogany Field. History matches were achieved under both volumetric depletion and weak water drive.
4. The recovery factors, predicted under current operating conditions, for volumetric versus weak water drive were 53% and 56%, respectively.
5. The recovery factors, predicted with compression, for volumetric versus weak water drive were 70% and 72%, respectively.
6. The higher recovery factor for water drive occurred because it was weak, allowing more reserves to be produced before abandonment pressure was reached, but not strong enough for the onset of high water cuts.
7. The addition of a horizontal gas well in the reservoir is anticipated to rate accelerate the reserves by 3.7 years under volumetric depletion and 4 years under water drive under current operating conditions.

Recommendations

The planned horizontal well should be added to the reservoir to rate accelerate reserves.

At least one additional well should be considered to mitigate the risk associated with the current two-well depletion of the reservoir.

Acknowledgements

The authors thank bpTT LLC for permission to publish this paper. Thanks also goes to Mike Mackow and the past and present members of the Mahogany Subsurface Team.

References

1. Lachance, D.P. and McCleary, N.R. “Offshore Mahogany Field Development to Support Trinidad’s LNG Plant”, paper OTC 10733 presented at 1999 Offshore Technology Conference, May 3-6.
2. Wood, L., “Chronostratigraphy and Technostratigraphy of the Columbus Basin, Eastern Offshore Trinidad”, AAPG Bulletin, 2000.
3. Pittman, E. D., “Relationship of Porosity and Permeability to Various Parameters Derived from Mercury Injection-Capillary Pressure Curves for Sandstone”, AAPG Bulletin (Feb. 1992), 191-8.
4. Dykstra, H. and Parsons, R.L., “The Prediction of Oil Recovery by Waterflood”, Secondary Recovery of Oil in the United States, 2nd ed., API (1950) 160-174.
5. Jensen, J.L., Lake, L.W., Corbett, P.W.M., Goggin, D.J.: *Statistics for Petroleum Engineers and Geoscientists*, Prentice Hall (1997) 46-48.
6. Amaefule, J. O., Altunbay, M., Djebbar, T., Kersey, D. G., Keelan, D. K., “Enhanced Reservoir Description: Using Core and Log Data to Identify Hydraulic (Flow) Units and Predict Permeability in Uncored Intervals/Wells”, paper SPE 26436 presented at 1993 SPE Annual Technical Conference and Exhibition, Houston, Texas, Oct. 3-6.
7. Gunter, G. W., Finneran, J. M., Hartman, D. J., Miller, J. D., “Early Determination of Reservoir Flow Units using an Integrated Petrophysical Model”, paper SPE 38970 presented at the 1997 SPE Annual Technical Conference and Exhibition, San Antonio, Texas, Oct. 5-8.
8. Ali-Nandalal, J., Staines, M., Bally, K., Finneran, J.M., “Optimal Locations and Performance Prediction of Horizontal Oil Wells in the Oil Rim at Mahogany, Offshore Trinidad”, Poster Session SPE 56814 presented at the 1999 SPE Annual Technical Conference and Exhibition, Houston, Texas, Oct. 3-6.
9. Doveton, J.H.: *Geologic Log Analysis Using Computer Methods*, AAPG Computer Applications in Geology No. 2, AAPG, Tulsa, OK (1994)169.
10. Albus, J.S., “A New Approach to Manipulator Control: The Cerebellar Model Articulation Controller (CMAC)”, Transactions of ASME (Sep. 1975) 220-227.
11. Hower, T.L. and Jones, R.E., “Predicting Recovery of Gas reservoirs Under Waterdrive Conditions”, paper SPE 22937 presented at 1991 Annual Technical Conference and Exhibition, Dallas, Texas, Oct. 6-9.

Table 1

Porosity Type	Intergranular macroporosity
Porosity Range	23-35 %
Permeability Range	47 to > 5000 mD
Average Water Saturation	20%
Shale Volume	5%
Net-to-Gross	0.77
Reservoir Pressure	4758 psi @ 9758 ft sstvd
Reservoir Temperature	172 degrees F @ 9758 sstvd
Gas Specific Gravity	0.59
Condensate API	47.9
Gas Viscosity	0.025
Gas Formation Volume Factor	1.0167
Drive Mechanism	Volumetric to date

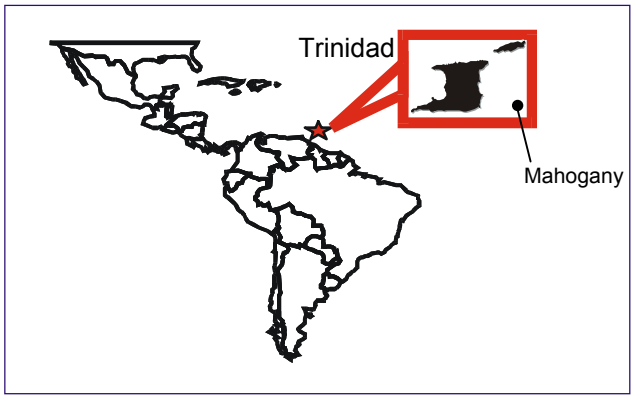

Figure 1 Location map for Mahogany Field

Table 2

Producing Well(s)	Drive Mechanism	Reserves (Bscf)	Recovery Factor (%)	Rate acceleration (years)
Current well	Volumetric Depletion	227	53	0
Current well	Water drive	239	56	0
Current well and horizontal 7” well	Volumetric Depletion	227	53	3.7
Current well and horizontal 7” well	Water drive	239	56	4.0
Current well and horizontal 7” well	Volumetric Depletion with Compression	301	70	5.5
Current well and horizontal 7” well	Water drive with Compression	310	72	5.7

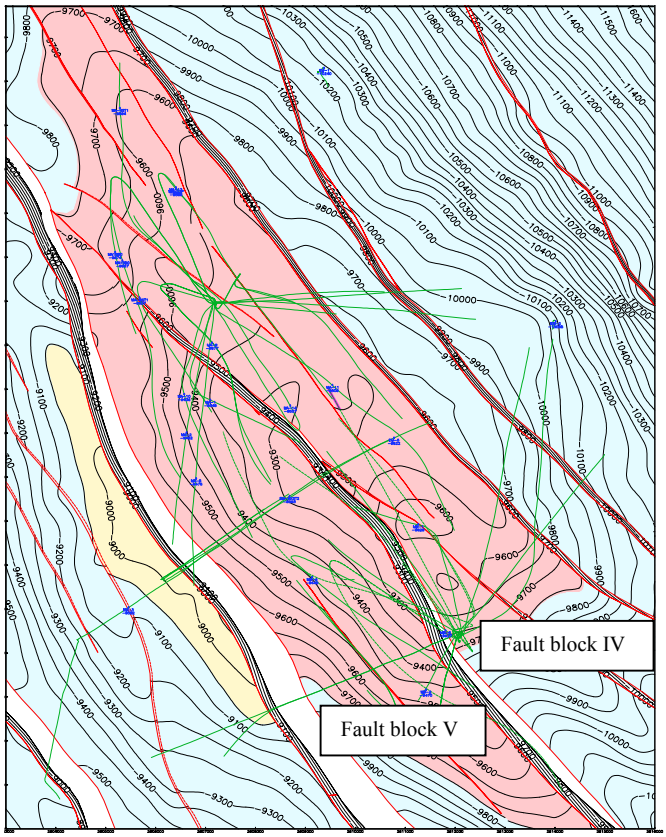

Figure 2 Structure map of the top of the 20 Sand showing fault block IV and V.

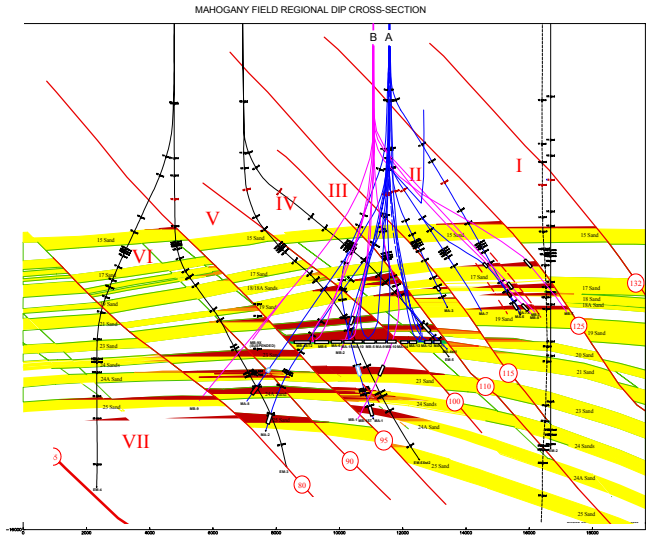

Figure 3 Cross section of Mahogany sands showing curved "bow-tie" shaped sequences.

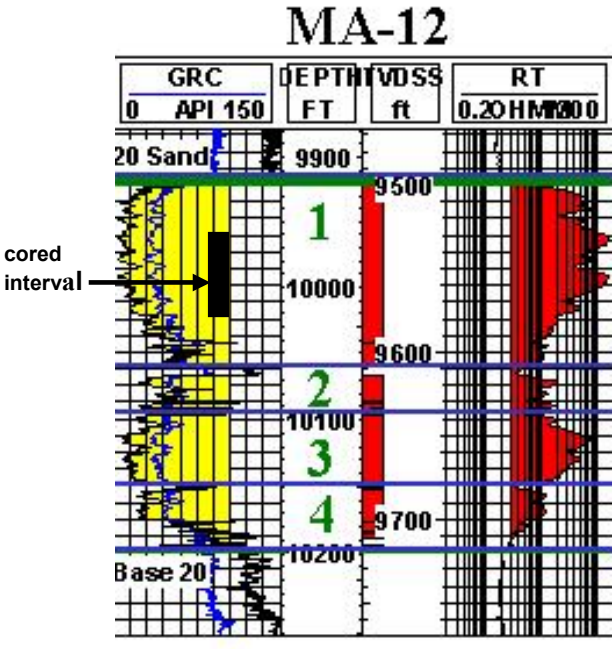

Figure 4 20 Sand is divided into four major stratigraphic units.

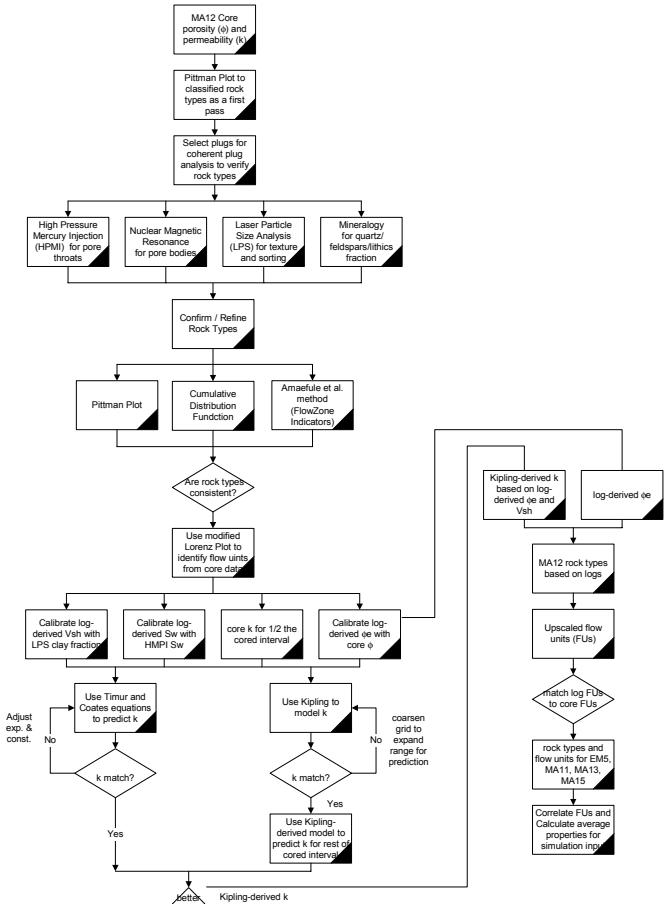

Figure 5 Work Flow to Calibrate Log to Core Data and Calculate Flow Unit Properties.

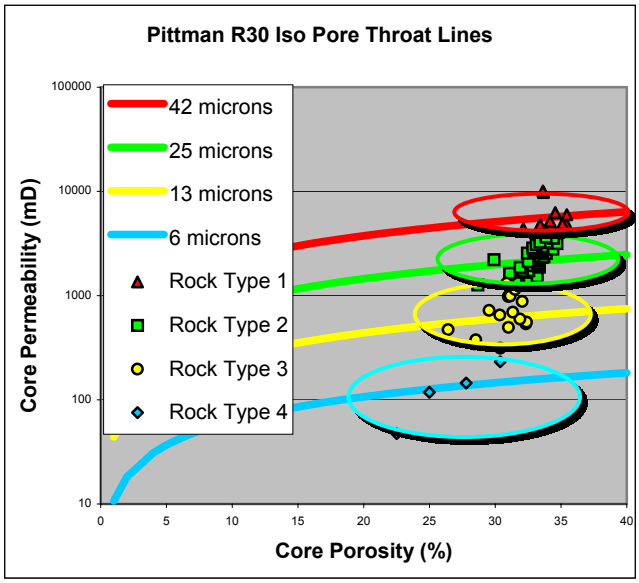

Figure 6 Pittman plot classified four rock types.

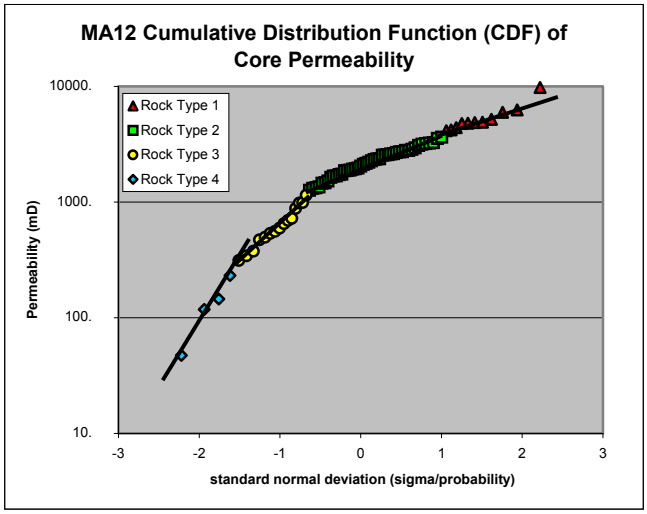

Figure 7 Cumulative Distribution Function distinguished four rock types associated with the four distinct slopes.

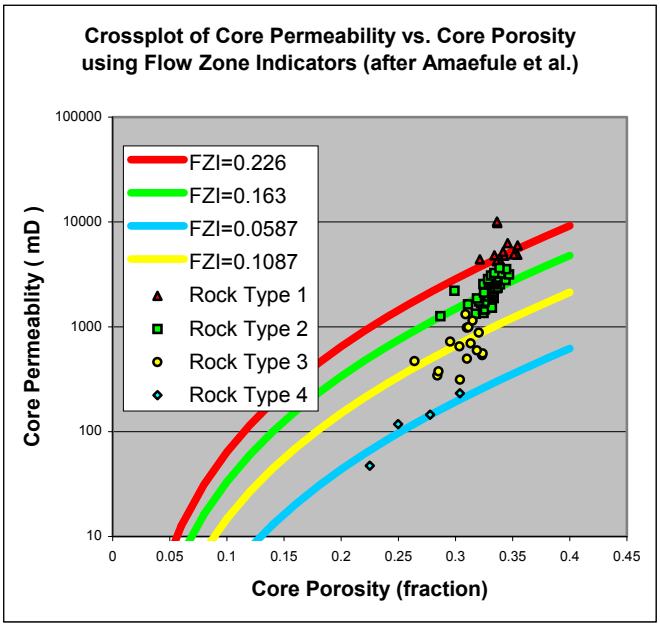

Figure 8A Four rock types were classified by the Amaefule et al. method using Flow Zone Indicators.

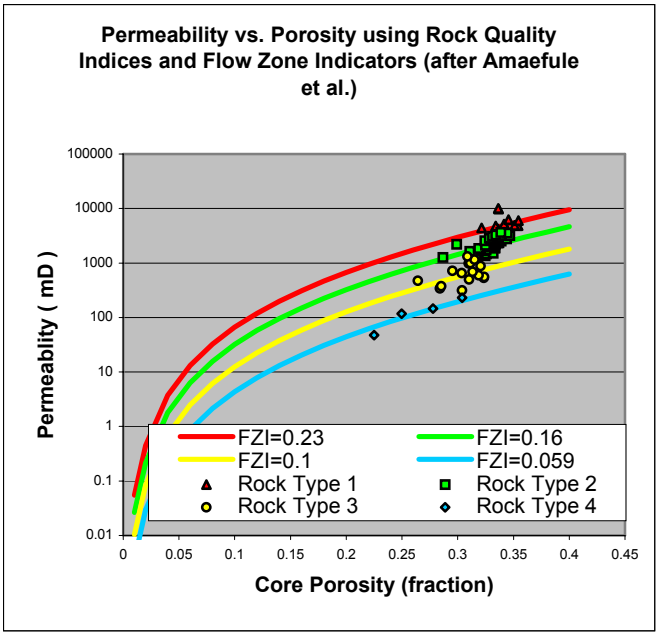

Figure 8B Four rock types are classified using Amaefule et al. method using the Rock Quality Index.

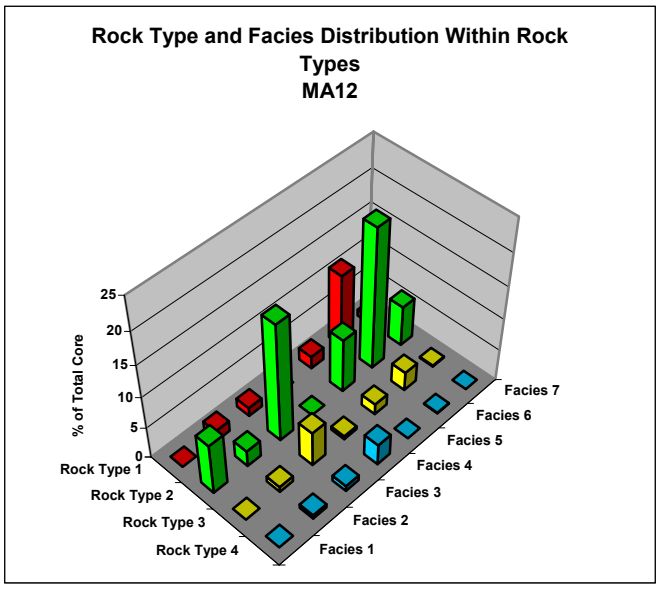

Figure 9 With the exception of Facies 1, there is no one-to-one relationship between rock type and facies. The majority of the core is composed of rock types 1 and 2.

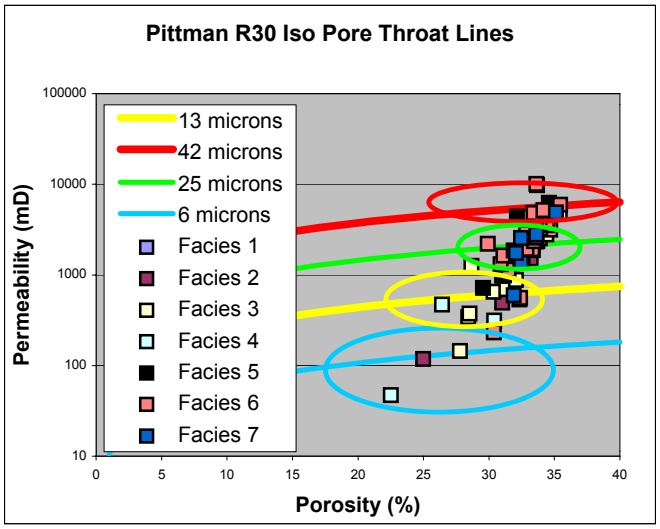

Figure 10 Facies shown on Pittman Plot.

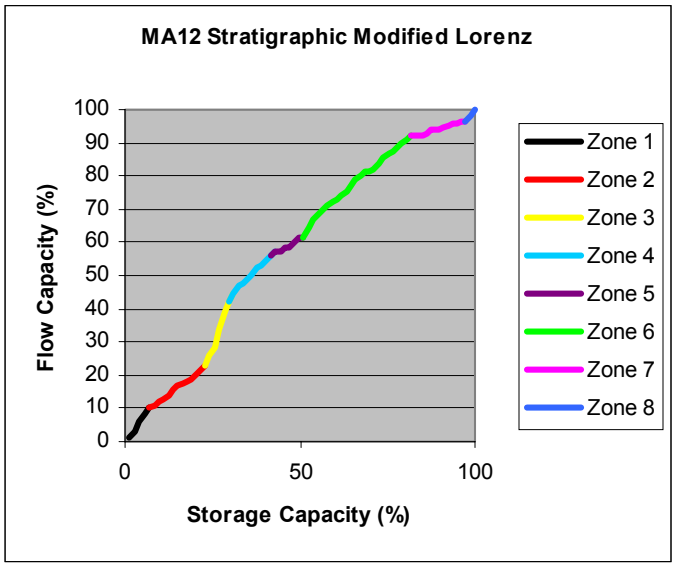

Figure 11 Stratigraphic modified Lorenz Plot identifying flow units from core data.

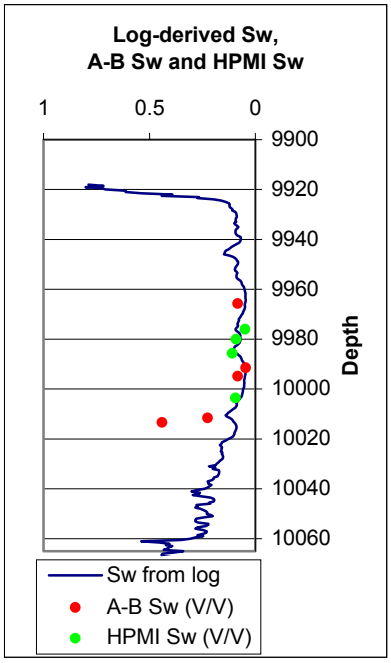

Figure 12 Log-derived Sw using Indonesian model matched Sw from high-pressure mercury injection and air brine capillary pressure measurements.

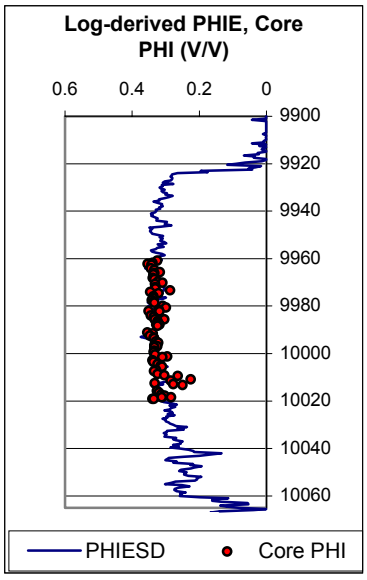

Figure 13 Log-derived porosity matched core porosity.

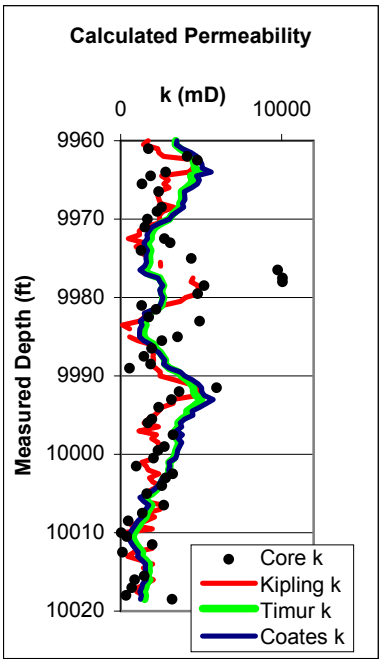

Independent test of permeability model

Figure 15 Calculated permeability compared to core permeability.

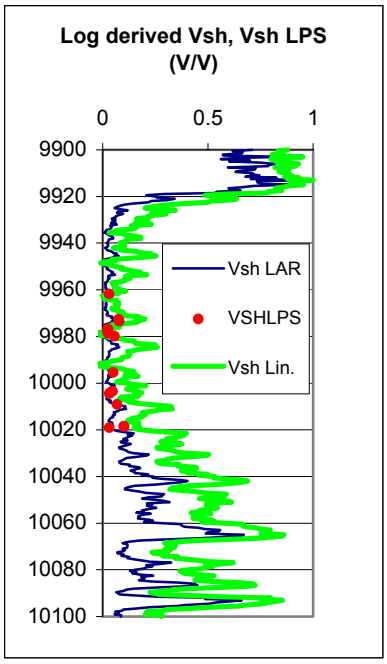

Figure 14 Vsh from linear and Larinov log calculations compared to Vsh from laser particle size analysis.

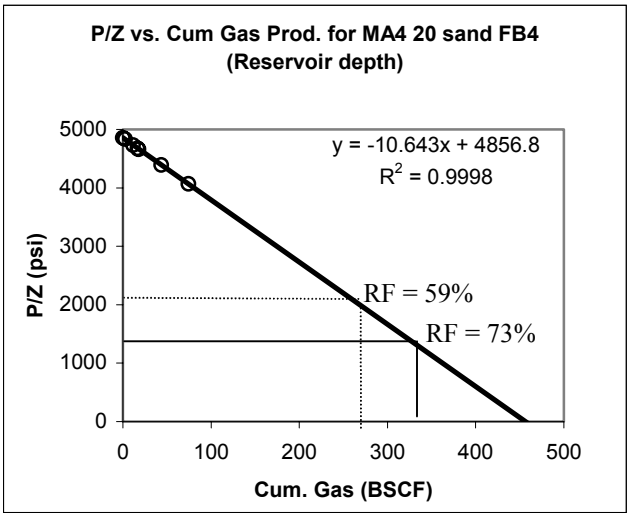

Figure 16 Material balance indicates volumetric drive is dominant production mechanism. Recovery at 2000 psi abandonment pressure was 59% whereas recovery with compression yields a recovery factor of 73% at an abandonment pressure of 1300 psi.

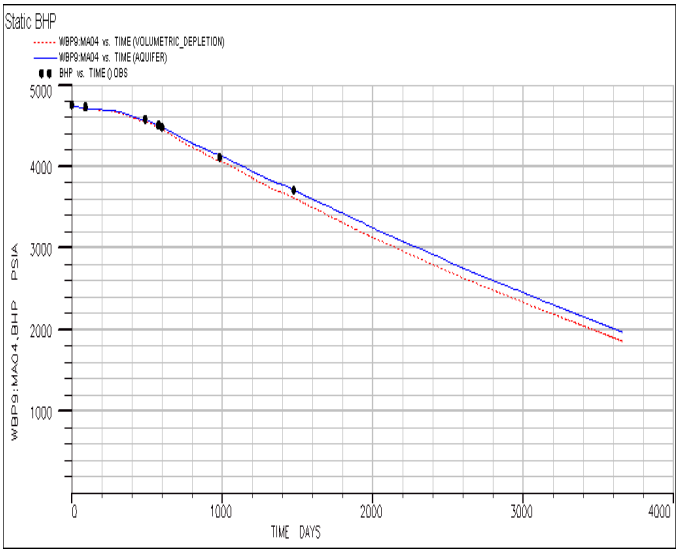

Figure 17A Static bottom hole pressure history match for volumetric and weak water drive cases.

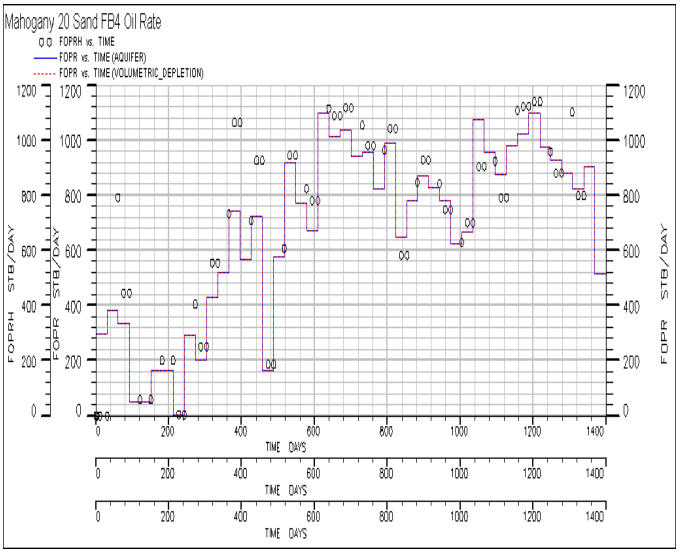

Figure 17C Condensate rate history match for volumetric and weak water drive cases.

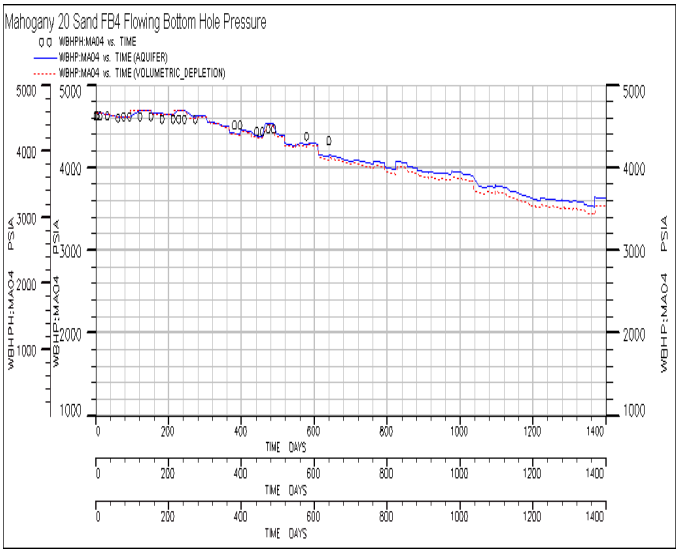

Figure 17B Flowing bottom hole pressure history match for volumetric and weak water drive cases.

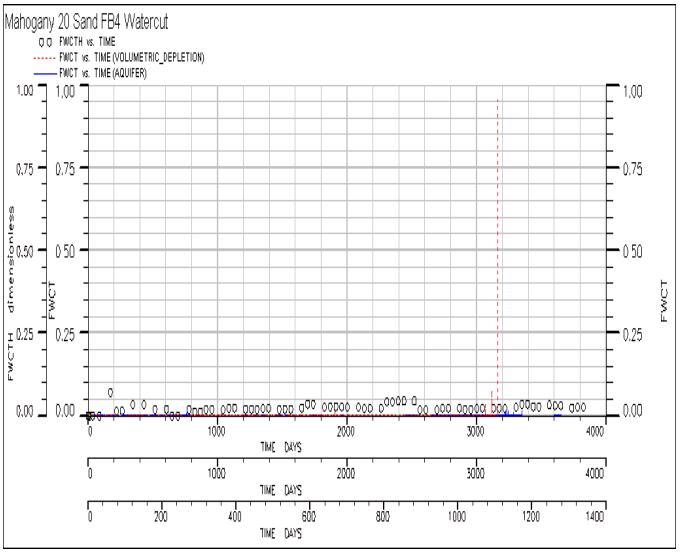

Figure 17D watercut history match for volumetric and weak water drive cases.

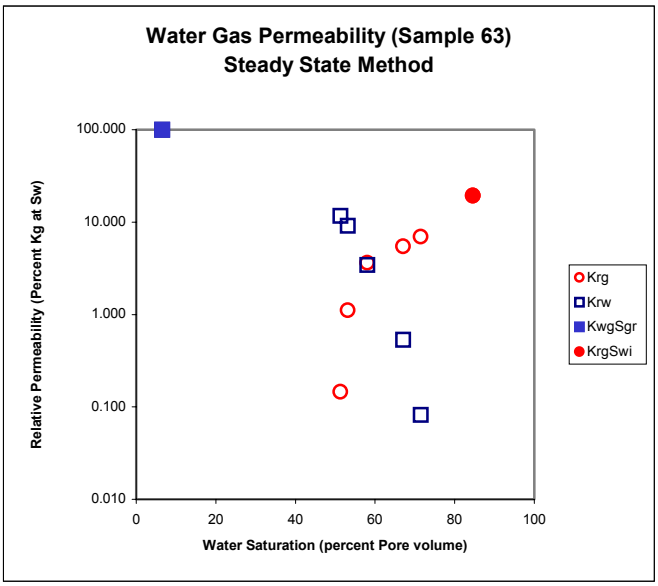

Figure 18 Gas-water relative permeability curve, showing that for a small increase in water saturation a large decrease in gas relative permeability is expected.